

7. P. PIETROKOWSKY, *Rev. Sci. Instrum.* **34** (1963) 445.  
 8. D. R. HARBUR, J. W. ANDERSON and W. J. MARAMAN, *Trans. Met. Soc. AIME* **245** (1969) 1055.  
 9. N. N. AULT, *J. Amer. Ceram. Soc.* **40** (1957) 69.

R. KREPSKI  
 K. SWYLER\*  
 H. R. CARLETON  
 H. HERMAN

*Department of Materials Science,  
 State University of New York,  
 Stony Brook, New York, USA*

Received 22 January  
 and accepted 3 February 1975

\*Present address: Brookhaven National Laboratory, Upton, New York, USA.

### *Attenuated total reflectance infra-red spectra of Portland cement*

The advantages of attenuated total reflectance (ATR) technique of infra-red spectrometry of cement materials have been emphasized in an earlier publication [1]. In order to establish the previous finding, six Portland cements of significantly variable composition have been studied by the ATR technique. The results of this analysis are presented in this short communication, to

(1) substantiate the characteristic band pattern of normal Portland cements in 1050 to 450  $\text{cm}^{-1}$  region, where the fundamental modes are known to appear,

(2) establish the reproducibility of ATR

spectra of Portland cements, and

(3) qualitatively assess the formation of relative proportions of tricalcium and dicalcium silicates in cements.

The ATR spectra of six Portland cement samples (NBS/SRM nos 633, 635, 636, 637, 638 and 1016) were taken on a KRS-5 crystal in an ATR attachment using a Perkin-Elmer 621 spectrometer. The critical angle of incidence of the radiation was maintained approximately at 40°. An ordinate scale expansion of  $\times 5$  was used in each case. The cements were used without any special treatment. Each sample was subjected to a repeated number of runs and one of the representative spectra of each sample has been reproduced in Fig. 1. The important bands have been listed in Table I. The accuracy of the

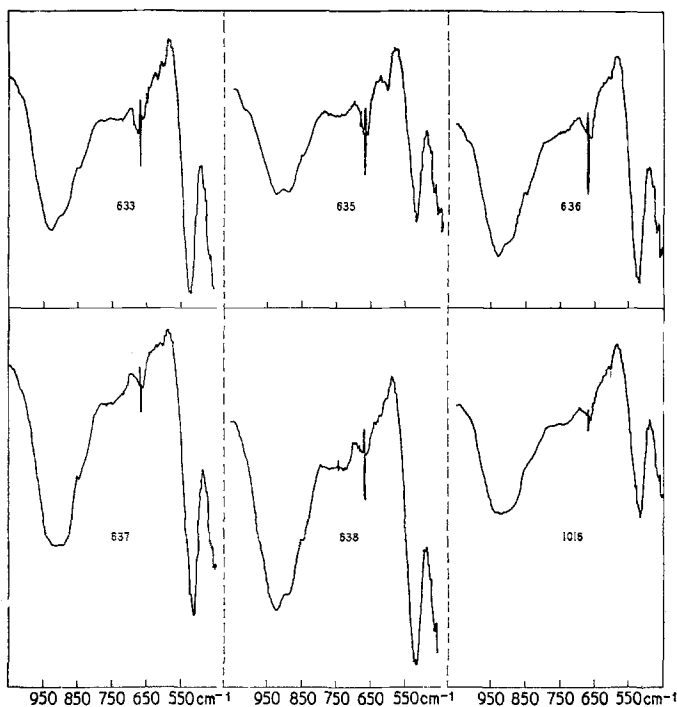


Figure 1 ATR infra-red spectra of Portland cements.

TABLE I Infra-red bands of Portland cements (cm<sup>-1</sup>)

NBS-633	930s,	898sh,	850sh	730w	620w,	600w	533sh,	524s,	520s	
NBS-635	923s,	890s,	846sh	750w	617w,	602w	533sh,	524sh,	517s	
NBS-636	930s,	910sh,	845sh	750w	620w,	603w	533sh,	527sh,	521s	
NBS-637	912s,	892s,	847sh	760w	618w,	600w		527sh,	515s	
NBS-638	923s,	892sh,	847sh	750w	618w,	601w		525sh,	519s	
NBS-1016	920s		850sh	748w		603w		532sh,	527sh,	520sh

s = strong, sh = shoulder, w = weak.

TABLE II Chemical and computed phase composition of cements

Major oxides and phases	Sample no.					
	633	635	636	637	638	1016
SiO <sub>2</sub>	21.90	18.50	23.20	23.10	21.40	21.05
Al <sub>2</sub> O <sub>3</sub>	3.74	6.20	3.10	3.30	4.50	4.97
Fe <sub>2</sub> O <sub>3</sub>	4.20	2.65	1.62	1.80	3.58	3.71
CaO	64.50	59.80	63.50	66.00	62.10	65.26
MgO	1.04	1.25	4.00	—	3.84	—
SO <sub>3</sub>	2.18	7.00	2.30	2.33	2.30	2.27
3CaO.SiO <sub>2</sub>	59.8	41.6	53.2	62.9	48.6	60.7
2CaO.SiO <sub>2</sub>	17.6	21.7	26.3	18.5	24.6	14.5
3CaO.Al <sub>2</sub> O <sub>3</sub>	2.7	12.2	5.4	5.7	5.7	7.0
4CaO.Al <sub>2</sub> O <sub>3</sub> .Fe <sub>2</sub> O <sub>3</sub>	12.6	7.8	4.9	5.3	11.2	11.2
CaSO <sub>4</sub>	3.5	11.8	3.9	3.9	3.9	3.8
C <sub>3</sub> S/C <sub>2</sub> S	3.4	1.9	2.0	3.4	2.0	4.1

band positions is within  $\pm 2$  cm<sup>-1</sup>.

If the composite cement spectra are compared with the individual spectra of the major constituent phases like C<sub>3</sub>S, C<sub>2</sub>S, C<sub>3</sub>A and C<sub>4</sub>AF\* [1], a shift in the positions of the band that are characteristic of the constituent phases is always observed. This may be ascribed to the difference in composition that originates due to solid solution and polymorphic transformations.

The spectra of all the cement samples are reproducible, particularly with respect to the general pattern, band positions, intensity and splitting. In the range 1050 to 450 cm<sup>-1</sup> the spectra are characterized by a strong and broad band in the region 1000 to 800 cm<sup>-1</sup>, which in general splits into two or three peaks, depending upon the presence of silicate phases in them. In the lower frequency range the spectra are characterized by a shallow ill-defined band in the 750 cm<sup>-1</sup> range followed by two small but sharp peaks in the 600 cm<sup>-1</sup> region and a strong band with the highest intensity which splits into two or three peaks in the 520 cm<sup>-1</sup> region. The sharp band at 667 cm<sup>-1</sup> is due to atmospheric carbon dioxide because of different path length induced by the ATR cell.

In the cement spectra, the frequency range 1000

\*C = CaO, S = SiO<sub>2</sub>, A = Al<sub>2</sub>O<sub>3</sub> and F = Fe<sub>2</sub>O<sub>3</sub>.

to 800 cm<sup>-1</sup> is the most important, so far as the silicate phases are concerned. The broad oxide composition and the calculated phase composition of the cement samples investigated are given in Table II. From this table it is obvious that the C<sub>3</sub>S/C<sub>2</sub>S ratio in sample no. 1016 is about 4, in samples 637 and 633 is about 3.4 and in the remaining samples it is in the neighbourhood of 2. If the corresponding spectra of these samples are compared it is observed that in sample no. 1016 with a C<sub>3</sub>S/C<sub>2</sub>S ratio of about 4 there is a strong band at 925 cm<sup>-1</sup> with no discernible splitting and a faint shoulder at 850 cm<sup>-1</sup>. In samples 637 and 633 with a C<sub>3</sub>S/C<sub>2</sub>S ratio of about 3.5, the band around 900 cm<sup>-1</sup> has split into two with comparatively more pronounced shoulders at 850 cm<sup>-1</sup>. Finally, in the remaining three samples with a C<sub>3</sub>S/C<sub>2</sub>S ratio of about 2, the above development is more pronounced. However, since in all the samples the proportion of C<sub>3</sub>S is predominant the band in the region 900 to 850 cm<sup>-1</sup> are less in intensity than the band beyond 900 cm<sup>-1</sup>. This confirms our earlier finding that the higher frequency band (>900 cm<sup>-1</sup>) corresponds to tricalcium silicate and the bands in the range of 900 to 850 cm<sup>-1</sup> owe their origin to the dicalcium silicate phase [1].

The broad diffused band in the region 750 to 700  $\text{cm}^{-1}$  may represent the aluminate and ferrite phases, as is evident from a pronounced peak in sample no. 635 containing about 20%  $\text{C}_3\text{A} + \text{C}_4\text{AF}$ .

The sharp and weak bands at 620 and 600  $\text{cm}^{-1}$  arise from calcium sulphate which is corroborated by the development of a better defined peak in sample no. 635 which contains considerably higher proportions of sulphate than the others.

The bands in the range 550 to 500  $\text{cm}^{-1}$  are produced as a result of superposition of characteristic bands of almost all the major cement minerals and hence have little value in the characterization of the composite material.

Based on this study, therefore, the following conclusions may be drawn.

(1) The ATR technique is suitable for infra-red spectrometry of cement materials.

(2) The ATR spectra of cements are resolved and reproducible.

(3) The splitting of the broad band in the frequency range 1000 to 800  $\text{cm}^{-1}$  could be used

as a satisfactory qualitative index regarding the relative proportions of the tricalcium and dicalcium silicate phases. It appears that the relative proportions of alite and belite may be predicted by matching in a computer any unknown cement spectra with the spectra of the constituent phases superimposed in different ratios.

(4) The shifting of the high frequency band may be accounted for by the different polymorphic forms of  $\text{C}_3\text{S}$  which are known to be stabilized by small amounts of impurities compared to  $\beta\text{-C}_2\text{S}$ .

### Reference

1. S. N. GHOSH and A. K. CHATTERJEE, *J. Mater. Sci.* **9** (1974) 1577.

Received 14 February  
and accepted 19 March 1975

S. N. GHOSH

A. K. CHATTERJEE

*Cement Research Institute of India,  
M-10 South Extension II, Ring Road,  
New Delhi, 110 049, India*

### Observation of twin faults in sputter-deposited high-purity nickel

Columnar grains with stacked microtwins were first observed in sputter-deposited copper [1]. Here, the conditions for formation of the microtwins in nickel and a comparison of the twinned microstructures in nickel and copper are described.

Nickel and copper deposits were made by d.c. triode sputtering, which is described elsewhere [1, 2]. The nickel sputtering target was made from a 3.8 cm diameter Materials Research Company MARZ Grade (99.995% pure) nickel rod. A 1.9 cm diameter rod of ASARCO Grade (99.999 + % pure) copper was pressed into a 4 cm diameter disc for the copper target. Nickel and copper deposits were made at nearly the same rate (average rate  $\sim 0.75 \mu\text{m min}^{-1}$ ) and at the same homologous deposition temperature  $T_H = 0.275$ , where  $T_H = T_D/T_M$ ;  $T_D$  is the deposition temperature (K) and  $T_M$  is the melting temperature (K). The substrate temperatures corresponding to  $T_H = 0.275$  were 473 K for nickel and 373 K for copper. The nickel and copper deposits were formed on metallographically polished copper and aluminium substrates, respectively,

which were 3.8 cm diameter. The deposits were made 2 to 4 mm thick so that cross-sections normal to the substrate plane could be studied.

Deposits were sliced normal to the substrate into 0.5 mm thick strips. A series of 3 mm diameter discs were punched from the strips so the deposits could be examined normal to the deposition direction by transmission electron microscopy. The nickel discs were thinned with 20% perchloric acid in ethyl alcohol at  $-10^\circ\text{C}$ , and the copper discs were thinned with 60% phosphoric acid in water at  $5^\circ\text{C}$  both using the jet thinning technique.

Columnar grains with stacked microtwins in sputtered nickel are shown by a dark-field micrograph obtained from a (002) diffraction spot (Fig. 1). Grain boundaries, such as A-A, were parallel to the growth direction. As with the copper deposits, the columnar grains in nickel grew with the [111] direction perpendicular to the substrate. The average grain-boundary spacing was  $0.38 \mu\text{m}$  which was about the same as the average spacing ( $0.4 \mu\text{m}$ ) observed for sputter-deposited copper shown in Fig. 2. Occasionally, as in copper [1], large spacings ( $> 2 \mu\text{m}$ ) were found for nickel. The similar grain-boundary spacings for nickel and